# Enhancing Scattering Circular Dichroism of Chiral Substrate via Mie Resonances

Hanqing Cai, Haifeng Hu, and Qiwen Zhan, *Senior Member, IEEE*

***Abstract*—Chirality plays a pivotal role in the interaction between light and matter, yet detecting chiral signals from natural materials remains a challenge, necessitating the enhancement of their intensity. In this study, we present an approach to investigate substrate chirality through exploiting light scattering from Mie particles. To comprehensively analyze the scattering phenomenon, we theoretically derive the T-matrix for a nonchiral Mie sphere positioned on a chiral substrate. Unlike the Mie sphere in free space, our derivation accounts for the intricate coupling between the scattered light by the sphere and the reflected light by the substrate. Employing the T-matrix framework, we calculate the scattering power and circular dichroism spectra. Our findings reveal a remarkable augmentation of chiral signals originating from the substrate, thanks to the Mie resonance within high-index spheres. This research underscores the feasibility of probing local chiral properties in the vicinity of a sample surface, promising new insights into chiral interactions at the nanoscale.**

***Index Terms*—Mie scattering, chirality, circular dichroism, T-matrix, high-index particle.**

## I. Introduction

CHIRALITY is a fundamental concept used to describe the degree of asymmetry in a three-dimensional object when subjected to mirror inversion. For instance, the human hand is a classic example of chirality, as each hand cannot be superimposed onto its mirror image. In the realm of chemical and biological molecules, their properties are intimately linked to their inherent chirality. Enantiomers, which are molecules with opposite chirality, often exhibit distinct pharmacological efficacies, highlighting the critical role that chirality plays in fields such as pharmacology and chemistry [1]. Chirality is a ubiquitous feature in the realm of biomolecules, playing a fundamental role in the intricacies of life. Biological molecules typically exhibit exclusive chirality, existing in either the left-handed (L-) or right-handed (D-) chiral form. Circular polarization at shorter wavelengths serves as a crucial tool for discerning and distinguishing chiral molecules, unraveling the mysteries of their interactions and functions [2]. Light fields themselves exhibit chirality, opening up the possibility of leveraging the chiral interaction between light and matter to discern the chirality of materials [3]. Circular dichroism (CD) stands as a widely adopted spectroscopic technique for determining the chirality of a sample. It achieves this by quantifying the disparity in light power between right-circularly polarized (RCP) and left-circularly polarized (LCP) light after passing through the chiral materials. However, CD signals often suffer from inherent weakness due to the fact that chiral molecules are significantly smaller in size than the wavelength of light. Consequently, distinguishing between them becomes a formidable challenge, particularly in the presence of environmental noise and optical measurement system artifacts.

Prior research has demonstrated the potential of utilizing surface-capped metal nanoparticles to augment and enhance chirality signals, offering a promising avenue for overcoming these limitations [4]. In the vicinity of plasmonic structures, it is possible to manipulate the local chirality of the optical field. Optical antenna theory can be harnessed to engineer chiral light [5], with the incorporation of chiral metals and organic materials enabling the creation of supramolecular glasses characterized by adjustable colors and circularly polarized luminescence [6]. In 2019, Rui et al. introduced the concept of symmetric metal-dielectric-metal (MDM) metamaterial structures as a means to amplify the chiral optical response resulting from the interaction between light and matter [7]. Recent demonstrations have illustrated that the integration of meta-surface design with perovskite nanostructures can give rise to innovative chiral perovskite meta-surfaces characterized by amplified chiral responses and heightened enantioselectivity [8]. Nonetheless, the intrinsic losses associated with metals can impact the practical performance of such materials. Consequently, in recent years, there has been a shift toward employing dielectric nanoparticles possessing high refractive indices for the precise manipulation of light fields at the nanoscale [9]. In 2018, a method was proposed to enhance light emission through a dielectric surface formed by periodic arrays of silicon nanoparticles, achieving efficient light emission enhancement by using the electromagnetic resonance effect of metasurfaces [10]. The nonlinear optical properties of individual silicon nanoparticles were harnessed to measure the

Manuscript received 16 October 2023; revised 28 November 2023; accepted 18 December 2023. Date of publication 29 December 2023; date of current version 5 January 2024. The work of Haifeng Hu was supported in part by the National Natural Science Foundation of China under Grant 62075132 and in part by the Natural Science Foundation of Shanghai under Grant 22ZR1443100. The work of Qiwen Zhan was supported in part by the National Natural Science Foundation of China under Grant 92050202 and in part by the Shanghai Science and Technology Committee under Grant 19060502500. *(Corresponding author: Haifeng Hu.)*

Hanqing Cai is with the School of Optical-Electrical and Computer Engineering, University of Shanghai for Science and Technology, Shanghai 200093, China (e-mail: 213330651@st.usst.edu.cn).

Haifeng Hu and Qiwen Zhan are with the School of Optical-Electrical and Computer Engineering, University of Shanghai for Science and Technology, Shanghai 200093, China, also with the Zhangjiang Laboratory, Shanghai 201204, China, and also with the Shanghai Key Lab of Modern Optical System, University of Shanghai for Science and Technology, Shanghai 200093, China (e-mail: hfhu@usst.edu.cn; qwzhan@usst.edu.cn).

Digital Object Identifier 10.1109/JPHOT.2023.3346310

intensity of the magnetic field in their vicinity [11]. Moreover, the advancement of chiral metamaterials has led to improved absorption and fluorescence emission characteristics in chiral molecules, enabling precise control over chiral interactions between light field and molecules, surpassing the capabilities of naturally occurring chiral light fields [12]. Wu et al. employed the T-matrix method to investigate the robust plasmon-induced interaction among chiral spherical particles [13]. Subsequently, Qu et al. delved into the interaction between high-order Bessel vortex beams and chiral particles [14]. Furthermore, precise control over the size and shape of silicon nanoparticles has allowed for the modulation of Mie resonances, thereby enhancing their optical performance [15]. By observing Mie scattering from suspended particles in water, the accurate inversion of particle size distribution information has become attainable [16]. More recently, T-matrix method is employed to analyze Mie scattering from chiral spheres under superchiral field illumination, revealing substantial enhancements in the chiral signal, attributed to the presence of Mie resonances [17]. Additionally, the study of the interaction mechanisms between light and Mie particles has yielded insights into new physical phenomena [18]. For instance, the excitation of anapole states within chiral Mie nanoparticles has demonstrated a remarkable enhancement in CD signal intensity [19]. In addition, chiral transfer can also effectively enhance the CD signal [20].

In this study, we introduce a theoretical model for quantifying chiral signals. Our approach involves the utilization of circularly polarized light to illuminate a non-chiral sphere positioned atop a chiral substrate, accounting comprehensively for the intricate interactions between the particle and the chiral substrate. We employ the T-matrix method to effectively analyze the scattering process. To accommodate the localized nature of the scattered light near the particle, we utilize an expansion technique with vector spherical harmonics and integrate it with the Fresnel reflection coefficients of the chiral substrate. Unlike previous approaches that relied on transmitted light to characterize and measure chiral responses, our method focuses on scattering light in proximity to the surface of chiral media. This approach minimizes the impact of absorption, which often occurs when light passes through the substrate. Moreover, our approach enables the derivation of accurate analytical solutions throughout the entire process. As a result, when compared to numerical methods, it offers a swifter and more precise computation of results.

## II. Theoretical Moedl

To solve the scattering problem, both the incident field and scattering field should be expanded as the sum of vector spherical harmonics (VSHs) [21]:

$$\mathbf{E}_{inc}(\mathbf{r}) = \sum_{n=1}^{+\infty}\sum_{m=-n}^{n} u_{mn}\mathbf{M}_{mn}^{(1)}(\mathbf{r}) + v_{mn}\mathbf{N}_{mn}^{(1)}(\mathbf{r}), \tag{1}$$

$$\mathbf{H}_{inc}(\mathbf{r}) = \frac{1}{iZ_0}\sum_{n=1}^{+\infty}\sum_{m=-n}^{n} u_{mn}\mathbf{N}_{mn}^{(1)}(\mathbf{r}) + v_{mn}\mathbf{M}_{mn}^{(1)}(\mathbf{r}), \tag{2}$$

$$\mathbf{E}_{s}(\mathbf{r}) = \sum_{n=1}^{+\infty}\sum_{m=-n}^{n} a_{mn}\mathbf{M}_{mn}^{(3)}(\mathbf{r}) + b_{mn}\mathbf{N}_{mn}^{(3)}(\mathbf{r}), \tag{3}$$

$$\mathbf{H}_{s}(\mathbf{r}) = \frac{1}{iZ_0}\sum_{n=1}^{+\infty}\sum_{m=-n}^{n} a_{mn}\mathbf{N}_{mn}^{(3)}(\mathbf{r}) + b_{mn}\mathbf{M}_{mn}^{(3)}(\mathbf{r}). \tag{4}$$

In (1)–(4), $\mathbf{r} = (r, \theta, \phi)$is the spatial coordinates. $Z_0$ is the vacuum impedance. $m$ and $n$ are orders of the VSHs. The functions $\mathbf{M}_{mn}^{(1)}(\mathbf{r})$ and $\mathbf{N}_{mn}^{(1)}(\mathbf{r})$ in (1) and (2) are VSHs with finite values at the origin, while the outgoing function $\mathbf{M}_{mn}^{(3)}(\mathbf{r})$ and $\mathbf{N}_{mn}^{(3)}(\mathbf{r})$ in (3) and (4) are used to ensure that the scattered field satisfies the radiation condition in far-field region. The expansion coefficients $u_{mn}$ and $v_{mn}$ can be determined for the specific incident field. Then the calculation of the scattering field is equivalent to solving scattering coefficients (i.e., $a_{mn}$ and $b_{mn}$). The connection between these two sets of coefficients can be characterized through the use of the T-matrix. In the case of a homogeneous and nonchiral sphere in free space, the T-matrix takes on a diagonal form, achieved by matching the boundary conditions at the surface of the sphere. ($r = R_s$). Therefore, the scattering problem can be directly solved by using the T-matrix [22].

$$\begin{bmatrix} \mathbf{E_s} \\ \mathbf{H_s} \end{bmatrix} = \mathbf{T}\begin{bmatrix} \mathbf{E}_{inc} \\ \mathbf{H}_{inc} \end{bmatrix}. \tag{5}$$

$\mathbf{T}$ is determined by the radius and optical parameters of sphere. The elements of T-matrix can be expressed as:

$$\mathbf{T}_{11} = \frac{Z_0\psi_n(k_0R_s)\psi'_n(k_1R_s) - Z_1\psi_n(k_1R_s)\psi'_n(k_0R_s)}{Z_1\psi_n(k_1R_s)\xi'_n(k_0R_s) - Z_0\xi_n(k_0R_s)\psi'_n(k_1R_s)}, \tag{6}$$

$$\mathbf{T}_{22} = \frac{Z_0\psi_n(k_1R_s)\psi'_n(k_0R_s) - Z_1\psi_n(k_0R_s)\psi'_n(k_1R_s)}{Z_1\xi_n(k_0R_s)\psi'_n(k_1R_s) - Z_0\psi_n(k_1R_s)\xi'_n(k_0R_s)}, \tag{7}$$

where the $\xi_n(x) = xh_x^{(1)}(x)$, $h_x^{(1)}(x)$ is the spherical Hankel function, $\psi_n$is the Riccati-Bessel function, $\psi'$ end $\xi'_n$ are respectively the derivatives of $\psi_n(x)$ and $\xi_n(x)$, $Z_0$ and $Z_1$ are wave impedance in free space and sphere, respectively.

This study takes into account the impact of substrate reflection on sphere scattering, necessitating a modification of the T-matrix for the scattering problem [23], [24], [25]. The multi-scattering process in this model is demonstrated in Fig. 1. Firstly, by using the T-matrix in free space, we can determine the primary scattering field, which can be expressed as the linear combination of VSHs [i.e., (1) and (2)]. The scattering field is partly reflected by the chiral substrate. Analytically, we calculate the reflected field for each vector spherical harmonic (VSH) component and expand the results using VSHs once more. Once all the reflected fields are acquired, we can recombine them to obtain the total reflected field, which also takes the form of a VSH field. Consequently, the reflection characteristics of the chiral substrate can be comprehensively described through a reflection matrix $\mathbf{L}_R$, and the reflected field can be expressed as $\mathbf{L}_R[\mathbf{E}_s, \mathbf{H}_s]^{\mathrm{T}}$ directly as shown in Fig. 1.

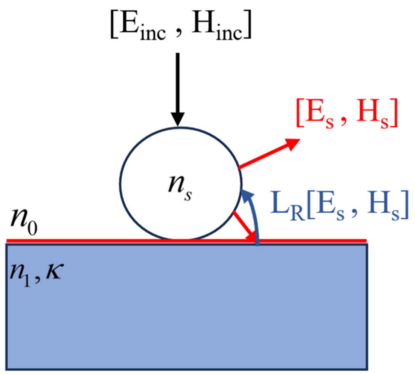


Fig. 1. Diagram illustrating the multiple scattering process by the Mie sphere on chiral substrate.

The interface will cause coupling between the reflected field from the substrate and the scattered field from the particle. In Fig. 1, The black and red arrows represent the path of the incident $[\mathbf{E}_{inc}, \mathbf{H}_{inc}]^{\mathrm{T}}$ and scattering light $[\mathbf{E}_s, \mathbf{H}_s]^{\mathrm{T}}$. The blue arrow represents the reflection of the scattering light by the substrate. When the primary scattering field is reflected back to the sphere, the secondary scattering field is excited. In this way, the total scattering field after multiple scattering and reflection processes can be expressed by (8) [25].

$$\begin{aligned}\begin{bmatrix}\mathbf{E_s}\\ \mathbf{H_s}\end{bmatrix} &= \sum_{\sigma=0}^{+\infty}(\mathbf{T}\mathbf{L}_R)^{\sigma}\mathbf{T}\begin{bmatrix}\mathbf{E}_{inc}\\ \mathbf{H}_{inc}\end{bmatrix}\\ &= (\mathbf{I}-\mathbf{T}\mathbf{L}_R)^{-1}\mathbf{T}\begin{bmatrix}\mathbf{E}_{inc}\\ \mathbf{H}_{inc}\end{bmatrix},\end{aligned} \tag{8}$$

therefore, in this problem, the effective T-matrix is:

$$\mathbf{T}_{eff} = (\mathbf{I}-\mathbf{T}\mathbf{L}_R)^{-1}\mathbf{T}, \tag{9}$$

where, $\mathbf{I}$ represents the unit matrix, $\mathbf{L}_R$ is the reflection operator of the chiral substrate, and $\mathbf{T}$ is the T-matrix for a sphere in free space.

Next, we will provide the precise expressions for the elements of the reflection matrix pertaining to the chiral interface. To achieve this, we will utilize the angular spectrum of vector spherical harmonics (VSHs) to account for reflection at the planar interface:

$$\begin{aligned}\mathbf{M}_{mn}^{(j)}(\mathbf{r}) &= \frac{(-i)^n\gamma_{mn}}{2\pi(1+\delta_{j,1})}\\ &\times\int_{\Omega_j} d\Omega_j e^{i\mathbf{k}\cdot\mathbf{r}}\left[im\pi_n^m(\theta)\hat{\theta}-\tau_n^m(\theta)\hat{\phi}\right]e^{im\phi},\end{aligned} \tag{10}$$

$$\begin{aligned}\mathbf{N}_{mn}^{(j)}(\mathbf{r}) &= \frac{(-i)^{n-1}\gamma_{mn}}{2\pi(1+\delta_{j,1})}\\ &\times\int_{\Omega_j} d\Omega_j e^{i\mathbf{k}\cdot\mathbf{r}}\left[\tau_n^m(\theta)\hat{\theta}+im\pi_n^m(\theta)\hat{\phi}\right]e^{im\phi},\end{aligned} \tag{11}$$

where $\mathbf{k}$ is the wave vector of the respective plane wave. The direction of a plane wave can be represented by $(\tilde{\theta}, \tilde{\varphi})$, where $\tilde{\theta}$ is the polar angle and $\tilde{\varphi}$ is the azimuthal angle of the wavevector. $\gamma_{mn}$ is a coefficient can be calculated by $(m, n)$:

$$\gamma_{mn} = \sqrt{\frac{(2n+1)(n-m)!}{4\pi n(n+1)(n+m)!}}, \tag{12}$$

$\pi_n^m(\theta)$ and $\tau_n^m(\theta)$ are represented as:

$$\pi_n^m(\theta) = \frac{mP_n^m(\cos\theta)}{\sin\theta}, \tag{13}$$

$$\tau_n^m(\theta) = \frac{dP_n^m(\cos\theta)}{d\theta}, \tag{14}$$

where $P_n^m$ is the associated Legendre function. Then, the reflection field should be considered by Fresnel reflection by the chiral interface. We suppose that an s-/p-polarized beam propagating in a homogeneous isotropic dielectric medium is incident at angle $\theta_i$ upon the surface of a chiral medium. The following constitutive relations of the chiral medium are used [26]:

$$\mathbf{D} = \varepsilon_1\mathbf{E} + i\kappa_1\mathbf{H}, \tag{15}$$

$$\mathbf{B} = \mu_1\mathbf{H} - i\kappa_1\mathbf{E}, \tag{16}$$

where $\kappa_1$ is the chirality parameter. $\varepsilon_1$ and $\mu_1$ are the relative permittivity and permeability of the chiral medium, respectively. In such a medium with chirality, the light beam splits into RCP and LCP with different phase velocity and refraction angles. As a result, upon entering the chiral media, the incident beams bifurcate into two transmitted waves: one right-handed circularly polarized wave (RCP) with phase velocity $\omega/k_+$ and one left-handed circularly polarized (LCP) wave with phase velocity $\omega/k_-$. Their wavevectors are given by $k_\pm = k_0 n_\pm$. The wavevectors in the vacuum are determined by the expression $k_0 = \omega/c$ and the index of the RCP/LCP wave is respectively $n_\pm = \sqrt{\varepsilon_1\mu_1} \pm \kappa_1$. Hence, the impact of the chiral substrate can be accounted for by applying the Fresnel reflection coefficients to each individual plane wave component in (10) and (11). Then the reflected VSHs can be expressed in (17) and (18):

$$\begin{aligned}\mathbf{M}_{mn,r}^{(j)} &= \frac{(-i)^n\gamma_{mn}}{2\pi\,(1+\delta_{1j})}\int_{\Omega_j} i\pi_n^m(\tilde{\theta})e^{im\tilde{\phi}}e^{2ik\cos\tilde{\theta}z_0}e^{i\mathbf{k}_R\cdot\mathbf{r}}\\ &\times\left(r_{\theta\theta}\hat{\theta}_{k_R}+r_{\theta\phi}\hat{\phi}_{k_R}\right)d\Omega\\ &-\frac{(-i)^n\gamma_{mn}}{2\pi\,(1+\delta_{1j})}\int_{\Omega_j}\tau_n^m(\tilde{\theta})e^{im\tilde{\phi}}e^{2ik\cos\tilde{\theta}z_0}e^{i\mathbf{k}_R\cdot\mathbf{r}}\\ &\times\left(r_{\phi\theta}\hat{\theta}_{k_R}+r_{\phi\phi}\hat{\phi}_{k_R}\right)d\Omega,\end{aligned} \tag{17}$$

$$\begin{aligned}\mathbf{N}_{mn,r}^{(j)} &= \frac{(-i)^{n-1}\gamma_{mn}}{2\pi\,(1+\delta_{1j})}\int_{\Omega_j}\tau_n^m(\tilde{\theta})e^{im\tilde{\phi}}e^{2ik\cos\tilde{\theta}z_0}e^{i\mathbf{k}_R\cdot\mathbf{r}}\\ &\times\left(r_{\theta\theta}\hat{\theta}_{k_R}+r_{\theta\phi}\hat{\phi}_{k_R}\right)d\Omega\\ &+\frac{(-i)^{n-1}\gamma_{mn}}{2\pi\,(1+\delta_{1j})}\int_{\Omega_j} i\pi_n^m(\tilde{\theta})e^{im\tilde{\phi}}e^{2ik\cos\tilde{\theta}z_0}e^{i\mathbf{k}_R\cdot\mathbf{r}}\\ &\times\left(r_{\phi\theta}\hat{\theta}_{k_R}+r_{\phi\phi}\hat{\phi}_{k_R}\right)d\Omega,\end{aligned} \tag{18}$$

where $\mathbf{k}_R$ is the wave vector of a reflected plane wave, and $z_0$ is the distance from the center of nanosphere to the substrate surface. In (17) and (18), we have used the Fresnel reflection coefficients for p-polarized and s-polarized light incident from normal media to chiral media [27]. The reflection coefficient of each plane wave can be calculated independently by the following equations:

$$r_{\theta\theta} = -\frac{\cos\theta_i(1-g^2)(\cos\theta_1+\cos\theta_2)-2g(\cos^2\theta_i-\cos\theta_1\cos\theta_2)}{\cos\theta_i(1+g^2)(\cos\theta_1+\cos\theta_2)+2g(\cos^2\theta_i+\cos\theta_1\cos\theta_2)}, \quad (19)$$

$$r_{\theta\phi} = \frac{2ig\cos\theta_i(\cos\theta_1-\cos\theta_2)}{\cos\theta_i(1+g^2)(\cos\theta_1+\cos\theta_2)+2g(\cos^2\theta_i+\cos\theta_1\cos\theta_2)}, \quad (20)$$

$$r_{\phi\theta} = \frac{-2ig\cos\theta_i(\cos\theta_1-\cos\theta_2)}{\cos\theta_i(1+g^2)(\cos\theta_1+\cos\theta_2)+2g(\cos^2\theta_i+\cos\theta_1\cos\theta_2)}, \quad (21)$$

$$r_{\phi\phi} = \frac{\cos\theta_i(1-g^2)(\cos\theta_1+\cos\theta_2)+2g(\cos^2\theta_i-\cos\theta_1\cos\theta_2)}{\cos\theta_i(1+g^2)(\cos\theta_1+\cos\theta_2)+2g(\cos^2\theta_i+\cos\theta_1\cos\theta_2)}. \quad (22)$$

Here $g=\sqrt{\varepsilon_1/\mu_1}$, $\theta_1$ and $\theta_2$ represent the refraction angle of the RCP and LCP waves in the chiral medium, which can be calculated by the law of refraction.

To calculate the elements of $\mathbf{L}_R$, the reflected fields have to be expended by the VSH basis, which has also been used to express the incident field of $[\mathbf{E}_{inc}, \mathbf{H}_{inc}]^{\mathrm{T}}$ in (1) and (2). The expansions of the reflected VSHs, $\mathbf{M}^{(j)}_{mn,r}$ and $\mathbf{N}^{(j)}_{mn,r}$ can be expressed as:

$$\mathbf{M}^{(j)}_{mn,r} = \sum_{\nu=1}^{+\infty}\sum_{\mu=-v}^{\nu}\left[A^{(j)}_{mn,\mu\nu}\mathbf{M}^{(1)}_{\mu\nu} + B^{(j)}_{mn,\mu\nu}\mathbf{N}^{(1)}_{\mu\nu}\right], \quad (23)$$

$$\mathbf{N}^{(j)}_{mn,r} = \sum_{\nu=1}^{+\infty}\sum_{\mu=-v}^{\nu}\left[C^{(j)}_{mn,\mu\nu}\mathbf{M}^{(1)}_{\mu\nu} + D^{(j)}_{mn,\mu\nu}\mathbf{N}^{(1)}_{\mu\nu}\right]. \quad (24)$$

Here, the expressions of the expansion coefficients are:

$$A^{(j)}_{mn,\mu\nu} = \delta_{\mu m}\frac{(-1)^m i^{\nu-n}\gamma_{mn}(2\nu+1)}{(1+\delta_{1j})\gamma_{m\nu}\nu(\nu+1)} \times \int_{C_j}\sin\tilde{\theta}d\tilde{\theta}e^{2ik\cos\tilde{\theta}z_0} \begin{bmatrix} m^2\pi^m_n(\tilde{\theta})\pi^{-m}_\nu(\tilde{\theta}_R)r_{\theta\theta} - im\pi^m_n(\tilde{\theta})\tau^{-m}_\nu(\tilde{\theta}_R)r_{\theta\phi} \\ +im\tau^m_n(\tilde{\theta})\pi^{-m}_\nu(\tilde{\theta}_R)r_{\phi\theta} + \tau^m_n(\tilde{\theta})\tau^{-m}_\nu(\tilde{\theta}_R)r_{\phi\phi} \end{bmatrix}, \quad (25)$$

$$B^{(j)}_{mn,\mu\nu} = \delta_{\mu m}\frac{(-1)^m i^{\nu-n}\gamma_{mn}(2\nu+1)}{(1+\delta_{1j})\gamma_{m\nu}\nu(\nu+1)} \times \int_{C_j}\sin\tilde{\theta}d\tilde{\theta}e^{2ik\cos\tilde{\theta}z_0} \begin{bmatrix} m\pi^m_n(\tilde{\theta})\tau^{-m}_\nu(\tilde{\theta}_R)r_{\theta\theta} - im^2\pi^m_n(\tilde{\theta})\pi^{-m}_\nu(\tilde{\theta}_R)r_{\theta\phi} \\ +i\tau^m_n(\tilde{\theta})\tau^{-m}_\nu(\tilde{\theta}_R)r_{\phi\theta} + m\tau^m_n(\tilde{\theta})\pi^{-m}_\nu(\tilde{\theta}_R)r_{\phi\phi} \end{bmatrix}, \quad (26)$$

$$C^{(j)}_{mn,\mu\nu} = \delta_{\mu m}\frac{(-1)^m i^{\nu-n}\gamma_{mn}(2\nu+1)}{(1+\delta_{1j})\gamma_{m\nu}\nu(\nu+1)} \times \int_{C_j}\sin\tilde{\theta}d\tilde{\theta}e^{2ik\cos\tilde{\theta}z_0} \begin{bmatrix} m\tau^m_n(\tilde{\theta})\pi^{-m}_\nu(\tilde{\theta}_R)r_{\theta\theta} - i\tau^m_n(\tilde{\theta})\tau^{-m}_\nu(\tilde{\theta}_R)r_{\theta\phi} \\ +im^2\pi^m_n(\tilde{\theta})\pi^{-m}_\nu(\tilde{\theta}_R)r_{\phi\theta} + m\pi^m_n(\tilde{\theta})\tau^{-m}_\nu(\tilde{\theta}_R)r_{\phi\phi} \end{bmatrix}, \quad (27)$$

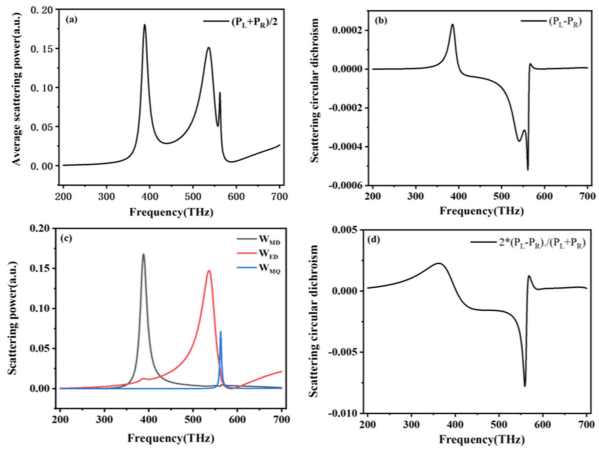


Fig. 2. (a) Average scattering power of nanosphere under the illumination of the LCP and RCP light. (b) Difference in scattering power under the illumination of the LCP and RCP light. (c) Contributions to the total scattering power from three different mechanisms, i.e., magnetic dipoles (MD), electric dipoles (ED), and magnetic quadrupoles (MQ). (d) Scattering CD spectrum of nanosphere.

$$D^{(j)}_{mn,\mu\nu} = \delta_{\mu m}\frac{(-1)^m i^{\nu-n}\gamma_{mn}(2\nu+1)}{(1+\delta_{1j})\gamma_{m\nu}\nu(\nu+1)} \times \int_{C_j}\sin\theta_k d\theta_k e^{2ik\cos\theta_k z_0} \begin{bmatrix} \tau^m_n(\tilde{\theta})\tau^{-m}_\nu(\tilde{\theta}_R)r_{\theta\theta} - im\tau^m_n(\tilde{\theta})\pi^{-m}_\nu(\tilde{\theta}_R)r_{\theta\phi} \\ +im\pi^m_n(\tilde{\theta})\tau^{-m}_\nu(\tilde{\theta}_R)r_{\phi\theta} + m^2\pi^m_n(\tilde{\theta})\pi^{-m}_\nu(\tilde{\theta}_R)r_{\phi\phi} \end{bmatrix}. \quad (28)$$

In (25)–(28), the integration range of $\tilde{\theta}$ is $[0, \pi/2 - i\infty]$.

After the expansion coefficients are obtained, the reflection matrix $\mathbf{L}_R$ can be represented as follows:

$$\mathbf{L}_R = \begin{bmatrix} A_{\mu\nu,mn} & B_{\mu\nu,mn} \\ C_{\mu\nu,mn} & D_{\mu\nu,mn} \end{bmatrix}. \quad (29)$$

We can use (23)–(28) to calculate the reflected matrix $\mathbf{L}_R$ for a chiral substrate. Then, the scattering coefficients $[a_{mn}, b_{mn}]^T$ can be calculated by (9). According to the classical Mie theory, the scattering power can be calculated by [21]:

$$P_{scat} = \frac{1}{2k_0^2}\sum_{n=1}^{+\infty}\sum_{m=-n}^{n}(|a_{mn}|^2 + |b_{mn}|^2). \quad (30)$$

## III. Results and Discussions

Subsequently, we conducted numerical simulations to validate the capacity of nonchiral Mie particles in probing the chirality of the substrate. In our model, the radius of Mie sphere is $R_s = 75$ nm, and refractive index is $n_s = 5$. The optical parameters of chiral substrate are $n_1 = 1.37$ and $\kappa_1 = 0.01$. The refractive index in free space is $n_0 = 1$.

The circularly polarized light is employed as incidence in this model. The scattering power under the illumination of LCP and RCP are represented by $P_L$ and $P_R$. In Fig. 2(a), the average scattering power $(P_L+P_R)/2$ are calculated in the frequency range of [200 THz, 700 THz]. According to multipole expansion method

[17], there are mainly three mechanisms during the scattering process, which are magnetic dipoles (MD), electric dipoles (ED), and magnetic quadrupoles (MQ) [24]. Their contributions to the scattering power can be calculated by (31)–(33):

$$W_{MD} = \frac{1}{2k_0^2}\sum_m |a_{m1}|^2, \tag{31}$$

$$W_{ED} = \frac{1}{2k_0^2}\sum_m |b_{m1}|^2, \tag{32}$$

$$W_{MQ} = \frac{1}{2k_0^2}\sum_m |a_{m2}|^2. \tag{33}$$

In Fig. 2(c), we computed the three scattering components to aid in elucidating the Mie resonance mechanism. It is evident that the three peaks in the scattering power spectrum shown in Fig. 2(a) correspond to the MD, ED, and MQ resonances, occurring at frequencies of 388.5 THz, 536 THz, and 562.5 THz, respectively. In Fig. 2(b), we calculated the difference in scattering power between $P_L$ and $P_R$. Notably, the presence of Mie resonance significantly enhances this scattering power difference. To quantify the chiral response of the model, we can calculate the scattering CD signal by $\mathrm{CD} = 2(P_L - P_R)/(P_L + P_R)$. In the CD curve presented in Fig. 2(d), two distinct regions exhibit enhanced CD signals. One region corresponds to the vicinity of the MD resonance wavelength, while the other is near the ED/MQ resonance wavelength. Intriguingly, the CD values in these two regions exhibit opposite signs. This observed fluctuation in chiral response can be elucidated by considering the alterations in the scattering mechanism of the chiral material at different wavelengths, which result in an inversion of the optical chiral response. In simpler terms, the scattering mechanism of a chiral material is wavelength-dependent. As the light frequency increases, the MD resonance can transition into ED and MQ resonances. The contrasting chiral responses can be attributed to the differing coupling properties between the Mie sphere and the chiral media, a phenomenon that can be analyzed using the reflection matrix as detailed in (29).

Then, we calculate the CD spectrum with different chiral parameters as illustrated in Fig. 3(a) and (b), when $\kappa_1 = -0.01$, 0.005, 0.01, 0.02, 0.05 and 0, respectively. As we can see in Fig. 3(a), when $\kappa_1 = 0$, the CD signal becomes zero, indicating the absence of chirality feature in the model. When $\kappa_1 = -0.01$ and 0.01, the scattering CD signals of left-handed and right-handed substrates have opposite signs. The intensity of CD signal can be enhanced at frequencies of 388.5 THz and 559 THz. Furthermore, as depicted in Fig. 3(b), we present CD curves for varying chiral parameters. These CD curves exhibit consistent trends but with varying intensities. To establish the correlation between substrate chirality and CD intensity, we concentrate on the chiral scattering analysis at frequencies of 388.5 THz and 559 THz. In Fig. 3(c), we calculate the scattering power under left-circularly polarized (LCP) and right-circularly polarized (RCP) incidences while altering the chiral parameter of the substrate within the range of [0, 0.05]. The corresponding CD curves are presented in Fig. 3(d). The linear relationship between

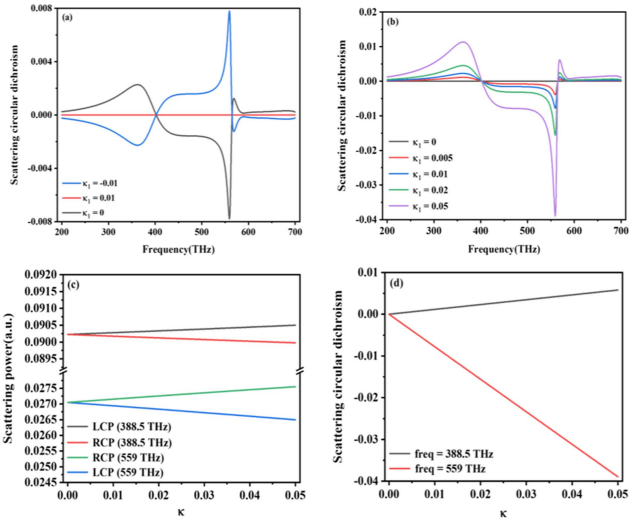


Fig. 3. (a) Scattering CD spectrum of a sphere on the chiral substrate under the illumination of the LCP and RCP light with $\kappa_1 = -0.01$, 0, and 0.01. (b) Scattering CD spectrum for $\kappa_1 = 0.005$, 0.01, 0.02, and 0.05. (c) Scattering power under the illumination of the LCP and RCP light at frequencies of 388.5 THz and 559 THz, respectively. (d) CD spectrum under the illumination of the LCP and RCP light at frequencies of 388.5 THz and 559 THz, respectively.

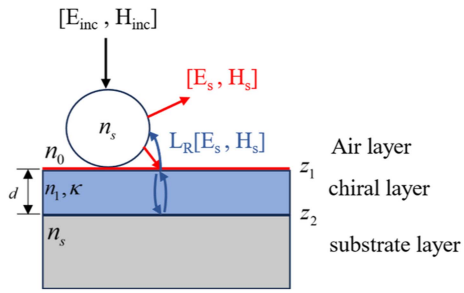


Fig. 4. Theoretical model for light scattering by Mie sphere on a chiral film, whose thickness is $d$ and refractive index is $n_1$. The positions of two interfaces of the chiral layer are $z = z_1$ and $z = z_2$.

the $\kappa$ value and CD intensity underscores the applicability of our proposed method for quantitative chirality measurement.

In the following, we consider a more realistic situation. A chiral film ($n_1$, $\kappa$) is coated on the achiral substrate ($n_s$), as illustrated in the Fig. 4. To consider the coupling between Mie scattering by high-index sphere and reflection by the chiral film, the reflection matrix for VSHs basis should be also calculated by (25)–(29). However, the reflection coefficients (i.e., $r_{\theta\theta}$, $r_{\theta\varphi}$, $r_{\varphi\theta}$, and $r_{\varphi\varphi}$) by the chiral film should be calculated by the transfer matrix of three-layer structure [26]. After the reflected light $\mathbf{L}_R\mathbf{E}_s$ is determined, effective T-matrix can be obtained by (9). Then the chiral scattering properties can be analyzed.

In the simulation, the thickness of chiral film is $d = 50$ nm. The refractive index of chiral film and substrate are 1.37 and 1.5. The chiral parameter of the film is $\kappa_s = 0.01$. Both left-handed and right-handed circularly polarized light are used for the incidence. In Fig. 5(a), we computed the average scattered power $(P_R + P_L)/2$ as shown by the red curve. As a comparison,

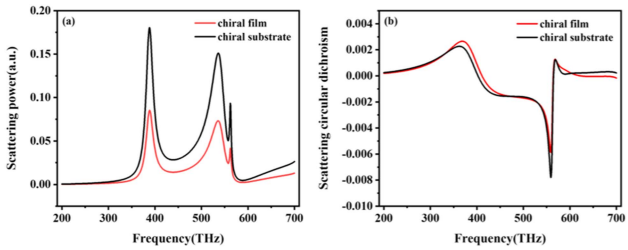


Fig. 5. (a) Average scattered powers for the Mie sphere on chiral film with $d = 50$ nm, $n_1 = 1.37$ and $\kappa_1 = 0.01$ (red curve) and chiral substrate with $n_s = 1.37$ and $\kappa_s = 0.01$ (black curve). (b) Spectra of CD signal for the chiral Mie scattering induced by chiral film and chiral substrate, respectively.

the results for Mie sphere on chiral substrate ($n_s = 1.37$. $\kappa = 0.01$) is shown by the black curve in Fig. 5(a). It can be evident that the scattered power for both the two cases exhibit the obvious Mie resonances at the same frequencies, but the scattering light intensity is reduced for the chiral film case. In Fig. 5(b), the CD signals are calculated by $P_R$ and $P_L$. It can be seen that the chiral film enhance the CD signal caused by MD resonance, while reduce the peak value of CD signal near the ED/MQ resonance.

## IV. Conclusion

We introduce a model to analyze the scattering of light by a Mie sphere situated on a chiral substrate within the theoretical framework of the T-matrix. The scattering power under left-circularly polarized (LCP) and right-circularly polarized (RCP) incidence offers insights into the properties of the chiral medium. Importantly, our approach mitigates the issue of light absorption, distinguishing it from traditional CD measurement that employ transmitted light to investigate substrate chirality. By employing a multipole expansion method, we provide a comprehensive explanation for the enhancement of chiral signals attributed to Mie resonance. Our theoretical analysis offers a plausible rationale for the regions of chiral enhancement, elucidating how the positive and negative peaks in CD spectrum reverse as the frequency increases, a phenomenon associated with the transition from magnetic dipole (MD) to electric dipole (ED). Furthermore, we also analyze the chiral Mie scattering induced by chiral film by the proposed method. Notably, our method hinges on rigorous analysis of the multi-scattering process. In contrast to conventional numerical techniques like finite element methods and finite-difference time-domain methods, our analytical approach ensures both precision and expedited computation speed, effectively extracting valuable information from the scattering field. This methodology establishes a robust foundation for investigating the interaction between chiral substrates and Mie particles.

## References

[1] G. A. Hembury, V. V. Borovkov, and Y. Inoue, "Chirality-sensing supramolecular systems," *Chem. Rev.*, vol. 108, no. 1, pp. 1–73, 2008.
[2] A. C. J. Bailey et al., "Circular polarization in StarFormation regions: Implications for biomolecular homochirality," *Science*, vol. 281, no. 5377, pp. 672–674, 1998.
[3] J. Mun et al., "Electromagnetic chirality: From fundamentals to nontraditional chiroptical phenomena," *Light Sci. Appl.*, vol. 9, 2020, Art. no. 139.
[4] M. Hentschel, M. Schäferling, X. Duan, H. Giessen, and N. Liu, "Chiral plasmonics," *Sci. Adv.*, vol. 3, no. 5, 2017, Art. no. e1602735.
[5] L. V. Poulikakos, P. Thureja, A. Stollmann, E. De Leo, and D. J. Norris, "Chiral light design and detection inspired by optical antenna theory," *Nano Lett.*, vol. 18, no. 8, pp. 4633–4640, 2018.
[6] F. Nie, K. Z. Wang, and D. Yan, "Supramolecular glasses with color-tunable circularly polarized afterglow through evaporation-induced self-assembly of chiral metal-organic complexes," *Nature Commun.*, vol. 14, no. 1, 2023, Art. no. 1654.
[7] G. Rui, H. Hu, M. Singer, Y. J. Jen, Q. Zhan, and Q. Gan, "Symmetric meta-absorber-induced superchirality," *Adv. Opt. Mater.*, vol. 7, no. 21, 2019, Art. no. 1901038.
[8] G. Long et al., "Perovskite metasurfaces with large superstructural chirality," *Nature Commun.*, vol. 13, no. 1, 2022, Art. no. 1551.
[9] A. I. Kuznetsov, A. E. Miroshnichenko, M. L. Brongersma, Y. S. Kivshar, and B. Luk'yanchuk, "Optically resonant dielectric nanostructures," *Science*, vol. 354, no. 6314, 2016, Art. no. aag2472.
[10] S. Murai, G. W. Castellanos, T. V. Raziman, A. G. Curto, and J. G. Rivas, "Enhanced light emission by magnetic and electric resonances in dielectric metasurfaces," *Adv. Opt. Mater.*, vol. 8, no. 16, 2020, Art. no. 1902024.
[11] G. C. Li et al., "Mapping the magnetic field intensity of light with the nonlinear optical emission of a silicon nanoparticle," *Nano Lett.*, vol. 21, no. 6, pp. 2453–2460, 2021.
[12] D. Ayuso et al., "Synthetic chiral light for efficient control of chiral light–matter interaction," *Nature Photon.*, vol. 13, no. 12, pp. 866–871, 2019.
[13] T. Wu, R. Wang, and X. Zhang, "Plasmon-induced strong interaction between chiral molecules and orbital angular momentum of light," *Sci. Rep.*, vol. 5, 2015, Art. no. 18003.
[14] T. Qu, Z. Wu, Q. Shang, J. Wu, and L. Bai, "Interactions of high-order Bessel vortex beam with a multilayered chiral sphere: Scattering and orbital angular momentum spectrum analysis," *J. Quantitative Spectrosc. Radiative Transfer*, vol. 217, pp. 363–372, 2018.
[15] C. Zhang et al., "Lighting up silicon nanoparticles with Mie resonances," *Nature Commun.*, vol. 9, no. 1, 2018, Art. no. 2964.
[16] H. Zhou and L. Li, "Experimental research on size distribution of suspended particles in water based on Mie scattering theory," *IOP Conf. Ser.: Earth Environ. Sci.*, vol. 769, no. 4, 2021, Art. no. 042063.
[17] H. Hu and Q. Zhan, "Enhanced chiral mie scattering by a dielectric sphere within a superchiral light field," *Physics*, vol. 3, no. 3, pp. 747–756, 2021.
[18] S. E. Svyakhovskiy, V. V. Ternovski, and M. I. Tribelsky, "Anapole: Its birth, life, and death," *Opt Exp.*, vol. 27, no. 17, pp. 23894–23904, 2019.
[19] H. Hu, Q. Gan, and Q. Zhan, "Achieving maximum scattering circular dichroism through the excitation of anapole states within chiral Mie nanospheres," *Phys. Rev. B*, vol. 105, no. 24, 2022, Art. no. 245412.
[20] E. Mohammadi, T. V. Raziman, and A. G. Curto, "Nanophotonic chirality transfer to dielectric Mie resonators," *Nano Lett.*, vol. 23, no. 9, pp. 3978–3984, May 10 2023.
[21] M. I. Mishchenko, L. D. Travis, and A. A. Lacis, *Lacis, Scattering, Absorption, and Emission of Light by Small Particles*. Cambridge, UK: NASA/Cambridge Univ. Press, 2002.
[22] A. G. Lamprianidis and A. E. Miroshnichenko, "Excitation of nonradiating magnetic anapole states with azimuthally polarized vector beams," *Beilstein J. Nanotechnol.*, vol. 9, pp. 1478–1490, 2018.
[23] M. A. Hernández-Acosta, L. Soto-Ruvalcaba, C. L. Martínez-González, M. Trejo-Valdez, and C. Torres-Torres, "Optical phase-change in plasmonic nanoparticles by a two-wave mixing," *Physica Scripta*, vol. 94, no. 12, 2019, Art. no. 125802.
[24] Y. Yang and S. I. Bozhevolnyi, "Nonradiating anapole states in nanophotonics: From fundamentals to applications," *Nanotechnology*, vol. 30, no. 20, 2019, Art. no. 204001.
[25] T. Bauer, S. Orlov, U. Peschel, P. Banzer, and G. Leuchs, "Nanointerferometric amplitude and phase reconstruction of tightly focused vector beams," *Nature Photon.*, vol. 8, no. 1, pp. 23–27, 2013.
[26] A. H. Sihvola, A. J. Viitanen, I. V. Lindell, and S. A. Tretyakov, *Electromagnetic Waves in Chiral and Bi-Isotropic Media*. Norwood, MA, USA: Artech House, 1994.
[27] H. Wang and X. Zhang, "Unusual spin Hall effect of a light beam in chiral metamaterials," *Phys. Rev. A*, vol. 83, no. 5, 2011, Art. no. 053820.